International Journal of Applied Earth Observation and Geoinformation 30 (2014) 30–41

Contents lists available at ScienceDirect

International Journal of Applied Earth Observation and Geoinformation

journal homepage: www.elsevier.com/locate/jag

Performance and effects of land cover type on synthetic surface reflectance data and NDVI estimates for assessment and monitoring of semi-arid rangeland

Edward M. Olexa[a,*], Rick L. Lawrence[b]

[a] U.S. Geological Survey, Northern Rocky Mountain Science Center, 2327 University Way, Suite 2, Bozeman, MT 59715, USA
[b] Department of Land Resources and Environmental Sciences, Montana State University, P.O. Box 173120, Bozeman, MT 59717, USA

ARTICLE INFO

Article history:
Received 24 August 2013
Accepted 15 January 2014

Keywords:
Landsat
MODIS
Rangeland
Remote sensing
STARFM

ABSTRACT

Federal land management agencies provide stewardship over much of the rangelands in the arid and semi-arid western United States, but they often lack data of the proper spatiotemporal resolution and extent needed to assess range conditions and monitor trends. Recent advances in the blending of complementary, remotely sensed data could provide public lands managers with the needed information. We applied the Spatial and Temporal Adaptive Reflectance Fusion Model (STARFM) to five Landsat TM and concurrent Terra MODIS scenes, and used pixel-based regression and difference image analyses to evaluate the quality of synthetic reflectance and NDVI products associated with semi-arid rangeland. Predicted red reflectance data consistently demonstrated higher accuracy, less bias, and stronger correlation with observed data than did analogous near-infrared (NIR) data. The accuracy of both bands tended to decline as the lag between base and prediction dates increased; however, mean absolute errors (MAE) were typically ≤10%. The quality of area-wide NDVI estimates was less consistent than either spectral band, although the MAE of estimates predicted using early season base pairs were ≤10% throughout the growing season. Correlation between known and predicted NDVI values and agreement with the 1:1 regression line tended to decline as the prediction lag increased. Further analyses of NDVI predictions, based on a 22 June base pair and stratified by land cover/land use (LCLU), revealed accurate estimates through the growing season; however, inter-class performance varied. This work demonstrates the successful application of the STARFM algorithm to semi-arid rangeland; however, we encourage evaluation of STARFM's performance on a per product basis, stratified by LCLU, with attention given to the influence of base pair selection and the impact of the time lag.

Published by Elsevier B.V.

1. Introduction

Society depends on the goods and services provided by healthy rangeland ecosystems. Proper functioning rangelands provide diverse ecosystem services, including water and nutrient cycling, biodiversity, climate regulation, recreation opportunities, and cultural heritage, in addition to the doctrinal role of forage production for wildlife and domestic livestock (James et al., 2003; Millennium Ecosystem Assessment, 2005). Permanent grassland pasture and rangelands comprise over one-fourth of the United States' land base and are second only to forestland in total acreage (Nickerson et al., 2011). The Bureau of Land Management (BLM) and the U.S. Forest Service (USFS) manage the majority of federally owned rangelands (National Research Council, 1994), including much of the 120 million hectares in arid and semi-arid regions of eight western states (Nickerson et al., 2011). Stewardship of these western rangelands requires condition assessment and trend monitoring using objective, detailed information about dynamic vegetation characteristics (Booth and Tueller, 2003; West, 2003) associated with local land cover and land use classes. Evaluating the influence of grazing on rangeland, however, is often problematic due to a lack of spatial and temporal data with sufficient resolution capable of revealing intra- and inter-annual patterns of vegetation response and changes in forage production at the sub-pasture level and across large extents (Blanco et al., 2009; Booth and Tueller, 2003; Bradley and O'Sullivan, 2011; West, 2003). These data limitations and insufficient resources allocated to monitoring rangeland vegetation (Fernandez-Gimenez et al., 2005) likely limit determination of the efficacy and duration of other management activities such as prescribed fire and chemical treatment of sagebrush (*Artemisia* spp.).

Data collected by a suite of previously active and currently extant earth observing satellites (EOS) can provide an efficient and cost effective alternative or addition to traditional field-based range evaluation methods (Eisfelder et al., 2012; Hunt and Miyake,

* Corresponding author. Tel.: +1 406 994 6269; fax: +1 406 994 6556.
E-mail address: eolexa@usgs.gov (E.M. Olexa).

0303-2434/$ – see front matter. Published by Elsevier B.V.
http://dx.doi.org/10.1016/j.jag.2014.01.008

2006; Pickup and Chewings, 1994; Ramsey et al., 2004). Remotely sensed (RS) data can be used to measure biophysical and phenological characteristics of vegetation at multiple spatiotemporal scales and extents (Coops et al., 2012; Jensen, 1983; Kerr and Ostrovsky, 2003; Washington-Allen et al., 2006). The potential application of these data, resultant vegetation indices, and RS-based classification and analysis techniques to rangeland management was recognized over half a century ago (Tueller, 1989); however, the utility of RS products depends on the information provided matching the needs of range managers (Hunt et al., 2003) and is largely influenced by satellite and sensor choice (Hunt et al., 2003; Kennedy et al., 2009; Turner et al., 2003).

RS data acquisition often requires a compromise among sensor and platform characteristics including spatial coverage, i.e., grain and extent, and temporal coverage as determined by its revisit interval and duration (Kennedy et al., 2009). Monitoring across large spatial extents at fine to moderate spatiotemporal scales has been impractical as no single satellite platform can provide the necessary data (Hansen et al., 2008; Singh, 2012). Landsat satellite series data have been used to investigate changes in land cover/land use (LCLU) at moderate spatial resolutions since the platform's initial launch in 1972 (Wulder et al., 2008), but a 16-day return interval often limits each sensor's ability to monitor dynamic conditions (Coops et al., 2012; Gao et al., 2006; Ju and Roy, 2008). The Terra and Aqua Moderate Resolution Imaging Spectroradiometer (MODIS) sensors provide large extent coverage with a daytime revisit cycle of 1–2 days (Gao et al., 2006), but their ≥250 m spatial resolution can limit their usefulness when evaluating habitat characteristics in spatially heterogeneous landscapes (Huete et al., 2002; Kennedy et al., 2009). Novel data integration methods seek to alleviate these limitations (Gao et al., 2006; Hansen et al., 2008; Hilker et al., 2009a; Zhu et al., 2010) and could facilitate monitoring seasonal and interannual changes in plant biomass and phenology across western rangelands by providing data tuned to the spatial and temporal resolution of traditional field based measurements (Hagen et al., 2012).

The integration, or fusion, of RS data from sensors with different spatial, temporal, or spectral characteristics seeks to produce additional or more refined information than is available from a single source (Pohl and van Genderen, 1998; Švab and Oštir, 2006). The suitability of blended data depends on their intended use and the fusion method employed. Traditional fusion techniques, i.e., color based and numerical or statistical (Pohl and van Genderen, 1998; Švab and Oštir, 2006), are often inappropriate when changes in surface reflectance or radiance values are evaluated. The Spatial and Temporal Adaptive Reflectance Fusion Model (STARFM) blends data provided by MODIS and Landsat sensors to produce synthetic imagery with the time-step of the MODIS input and surface reflectance values at 30 m spatial resolution (Gao et al., 2006). The STARFM algorithm predicts pixel reflectance values based on spatially and spectrally weighted differences between concurrent paired Landsat and MODIS scenes and a MODIS image collected on the prediction day (Gao et al., 2006). STARFM is not restricted to MODIS and Landsat imagery, but use of other data appears to have been rarely reported (but see Liu and Weng, 2012).

Initial research demonstrated STARFM's ability to successfully predict surface reflectance values at Enhanced Thematic Mapper Plus (ETM+) resolution for homogeneous landscapes consisting of forest and cropland and heterogeneous forest–cropland composites (Gao et al., 2006). Subsequent use of synthetic imagery time series effectively revealed seasonal changes in relative biomass (Hilker et al., 2009b) and mapped forest disturbance (Hilker et al., 2009a). The effectiveness of the STARFM algorithm depends strongly on the number of homogeneous coarse-resolution pixels in the study area and could be limited in spatially heterogeneous areas with patch sizes smaller than the MODIS input (Gao et al., 2006). Application of STARFM to varied, non-forest dominated landscapes remains limited (Emelyanova et al., 2012; Schmidt et al., 2012; Singh, 2011), and the algorithm is untested on semi-arid shrub-steppe dominated rangelands common to the western United States (but see Walker et al., 2012). The Enhanced Spatial and Temporal Adaptive Reflectance Fusion Model (ESTARFM) was developed to provide more accurate reflectance estimates in complex landscapes, but it requires at least two pairs of input images and is often less accurate than the original STARFM algorithm (Emelyanova et al., 2012; Zhu et al., 2010). The original STARFM could prove more useful when it is difficult or not possible to acquire more than one input pair or when the prediction date occurs beyond the temporal extent of available input pairs.

This study investigated the ability of the STARFM algorithm to predict surface reflectance and examined the quality of normalized difference vegetation index (NDVI) estimates associated with a heterogeneous dryland region of the western United States. We assessed STARFM's performance when applied to the entire study area, as well as for key LCLU classes, using pixel-based correlation analyses and examination of difference images of observed and predicted data. Spectral quality was evaluated on a bandwise basis for the red and NIR bands and for NDVI (Rouse et al., 1974) data derived from the predicted reflectance values. The influence of input pair selection on prediction quality was also assessed, but, unlike previous studies (Walker et al., 2012), we utilized the full set of available TM-MODIS image pairs to investigate the time lag and base pair effects.

2. Methods

2.1. Study area

The study area was delineated by the intersection of five Landsat scenes (path 38 row 31) and covers nearly 33,600 km^2, including portions of Idaho, Utah, and Wyoming (Fig. 1). Extensive parts of the Wyoming Basins and Utah-Wyoming Rocky Mountains ecoregions and small segments of the Columbia Plateau and Great Basin Ecoregions are represented (Andelman et al., 1999; Bailey, 1995; Freilich et al., 2001; Nachlinger et al., 2001; Noss et al., 2001). Shrubland, steppe, and savanna ecological systems (Comer et al., 2003) represent over 43% of the area. In contrast, human development and forest/woodland systems comprise 14% and 21% of the area, respectively. The Columbia Plateau, Great Basin, and Wyoming Basins rank as the top three in extent of sagebrush cover among all western ecoregions, and the Utah-Wyoming Rocky Mountains and Wyoming Basins ecoregions provide over 20% of the nation's sagebrush (Rowland and Leu, 2011). Elevation ranges from 1276 m above sea level at the Great Salt Lake to >3500 m in the Uinta Mountains. The long winters and short hot summers typical of cold continental weather patterns are prevalent in the Wyoming Basins ecoregion (Rowland and Leu, 2011); however, the timing and amount of precipitation is highly variable spatially and seasonally. The mountain ranges of the Utah-Wyoming Rocky Mountains ecoregion receive considerable winter precipitation, but much of the area is considered arid or semi-arid (Rowland and Leu, 2011). Total annual precipitation varies from a low of approximately 160 mm west of the Little Colorado Desert, Wyoming, to >1840 mm in the Wasatch Range in Utah (PRISM Climate Group, 2007). Species distribution and richness is influenced by the interaction of regional climatic conditions and local topographic features, e.g., elevation, aspect, and juxtaposition relative to mountain ranges (Noss et al., 2001).

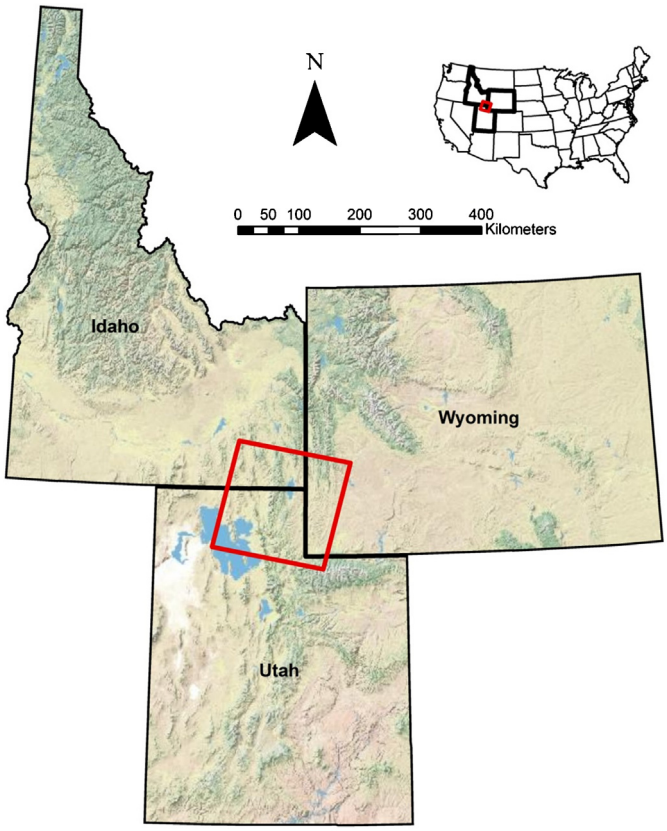

Fig. 1. Location of study area (red polygon) defined by the common extent of five Landsat 5 TM scenes (path 38 row 31) recorded in 2006.

2.2. Satellite data

Five Landsat TM scenes (path 38 row 31) collected on 6 June, 22 June, 09 August, 26 September, and 12 October 2006 and five Terra MODIS images (horizontal 09 vertical 04) collected on 5 June, 23 June, 10 August, 25 September, and 12 October 2006 were obtained from the U.S. Geological Survey (USGS) Center for Earth Resources Observation and Science Center (EROS) following preliminary visual inspection to ensure minimal cloud-cover. All TM images were processed to Level 1T, i.e., systematic radiometric and geometric corrections applied, prior to retrieval via the GLOVIS portal (http://glovis.usgs.gov). Digital numbers (DN) were converted to at-surface reflectance values using visual and histogram based outlier identification to determine minimum DN values, sensor specific radiometric calibration coefficients (Chander et al., 2009), and an image-based atmospheric correction model (Chavez, 1996). Visual inspection confirmed near perfect alignment of all TM scenes and ensured co-registration (RMSE $\leq$0.5 pixel) with a base image collected on 06 June 2006.

Scene selection ensured MODIS 250 m daily reflectance products (MOD09GQ) were spatially and temporally coincident with the TM imagery and produced a series of scenes with minimal cloud-cover that spanned the majority of the growing season (May–October). We utilized MODIS data collected within one day of TM scene acquisition when necessary to avoid images containing anomalies caused by directional reflectance differences associated with the junction of MODIS overpasses. We reprojected all MODIS scenes from Sinusoidal to UTM zone 12, resampled to 30 m resolution using the nearest neighbor method, and spatially and spectrally subset each scene using the MODIS Reprojection Tool (Release 4.0). Co-registration of all MODIS imagery was ensured and alignment of TM and MODIS imagery was evaluated by visual inspection of readily identifiable features.

All RS imagery was further spatially and spectrally subset to produce single layer red and NIR scenes with a common spatial extent defined by the footprint of the TM scenes. Geospatial Data Abstraction Library (GDAL, 2011) command line utilities translated all imagery to generic binary format and TM reflectance data were rescaled to unsigned 16 bit with a scale factor of 10,000 per STARFM requirements.

2.3. The STARFM algorithm and image fusion

The STARFM algorithm produces synthetic surface reflectance data from a base pair of TM and MODIS images and a single MODIS scene collected on the prediction date. The relationship between measured Landsat and MODIS surface reflectance values at pixel location (x_i, y_j) collected on the same date (t_0) is described as

$$L(x_i, y_j, t_0) = M(x_i, y_j, t_0) + \varepsilon_0 \quad (1)$$

where ε_0 is the difference between observed Landsat and MODIS reflectance values (Gao et al., 2006). If the difference between observed Landsat and MODIS reflectance values remains constant between the base date (t_0) and prediction date (t_k), Landsat surface reflectance values are estimated (Gao et al., 2006) by

$$L(x_i, y_j, t_k) = M(x_i, y_j, t_k) + L(x_i, y_j, t_0) - M(x_i, y_j, t_0). \quad (2)$$

However, changes in land cover type and phenology, heterogeneity in resampled MODIS pixels, and MODIS bidirectional reflectance distribution function (BRDF) changes can lead to variation in ε_0 and interfere with accurate estimation of Landsat reflectance values (Gao et al., 2006). Incorporating information from neighboring, spectrally similar pixels reduces the influence exerted by ε_0. Reflectance values are calculated using the weighting function W_{ij} that accounts for the spectral difference between Landsat and MODIS pixel data, changes between MODIS data recorded at t_0 and t_k, and the distance between the central pixel and the neighboring pixels (Gao et al., 2006) according to

$$L(x_{w/2}, y_{w/2}, t_k) = \sum_{i=1}^{w}\sum_{j=1}^{w} W_{ij} \times (M(x_i, y_j, t_k) + L(x_i, y_j, t_0) - M(x_i, y_j, t_0)) \quad (3)$$

where L is the reflectance value at the central pixel of a moving window of size w predicted for time t_k. Details concerning the development of the weighting function are provided elsewhere (Gao et al., 2006).

We applied the STARFM algorithm (version 1.1.2) (Gao et al., 2006) to five image pairs comprised of concurrent Landsat TM and Terra MODIS scenes recorded during the 2006 growing season. Twenty synthetic scenes were produced by using each image pair (Fig. 2) as the input base pair to predict reflectance data for the remaining four dates. We predicted reflectance data separately for the red and NIR bands using control parameters consistent with previous studies to enable comparisons to those studies without the confounding effects of different control parameters. Input parameters included a moving search window of 1500 m $\times$ 1500 m centered on each pixel, surface reflectance uncertainties of 0.002 for red and 0.005 for NIR, spectral similarity based on 40 classes defined for each pixel contingent on the standard deviation of the fine resolution reflectance data, and 2% as the minimum threshold of valid samples required within the search window. Large bodies of water, their adjacent littoral areas, and cloud contaminated areas were visually identified, screen digitized to include a variable width buffer, and classified as no data. The prediction quality of each reflectance band was evaluated using the resulting datasets.

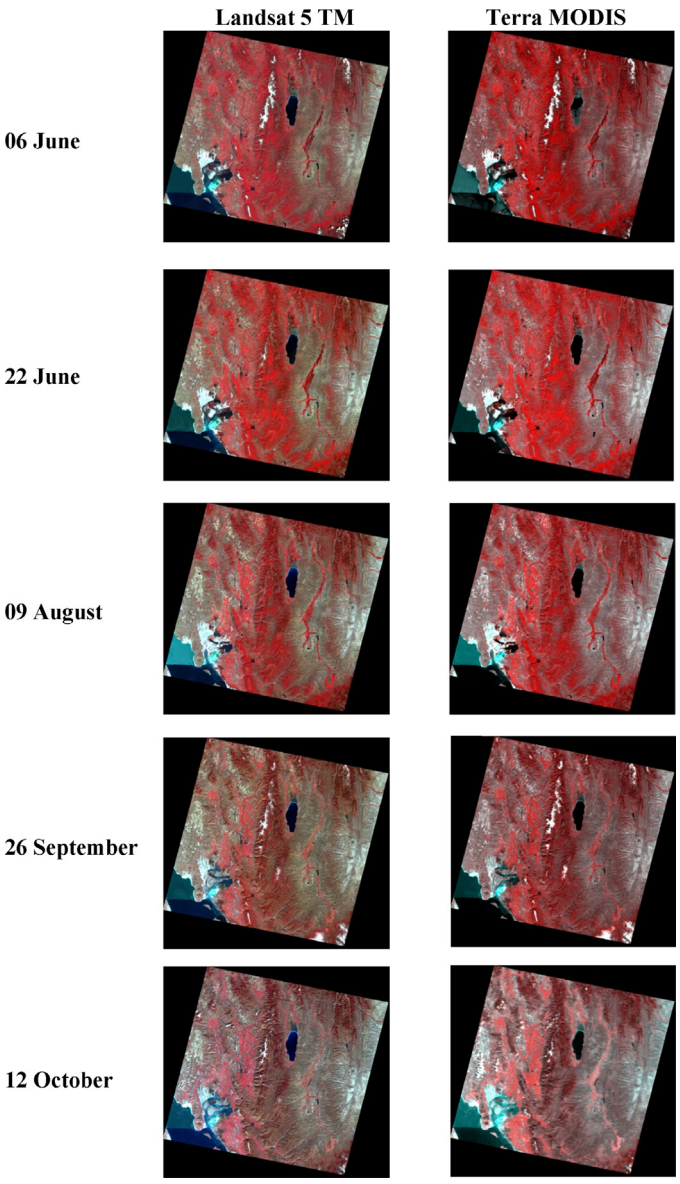

Fig. 2. False-color IR Landsat 5 TM and Terra MODIS image pairs recorded in 2006 and used to predict red and NIR surface reflectance using the STARFM algorithm. Each image pair was used to produce reflectance estimates for the other four days. Each image pair is labeled by the collection date of the TM image.

NDVI data were calculated for each prediction date as the ratio of the difference between the NIR and red reflectance estimates and their sum (Rouse et al., 1974). Our study design permitted the investigation of multiple aspects of image fusion including the influence of base pair selection, the effect of the time lag between base and prediction dates, and the influence of the chronological order of the base and prediction dates.

2.4. Quality assessment of synthetic reflectance and NDVI data

We assessed the quality of synthetic reflectance and NDVI data with pixel-based comparisons of observed and predicted values and simple linear regression-based correlation analysis. This approach permitted evaluation of the effectiveness of the STARFM algorithm when applied to semi-arid rangeland and comparison to similar studies (Hilker et al., 2009b; Schmidt et al., 2012; Walker et al., 2012; Zhu et al., 2010). Mean differences and MAE values indicated the relative bias and accuracy of predicted values, respectively, and were based on the full datasets to preclude sampling uncertainty. The standard deviations of the raw errors served to measure precision. Additionally, we stratified the NDVI data using 10 common LCLU classes (Comer et al., 2003) prior to examining for variations in prediction quality associated with cover and land use. All analyses utilized the R software environment (R Development Core Team, 2011) and the package "raster" (Hijmans and van Etten, 2011).

3. Results

3.1. Area-wide reflectance and NDVI predictions

3.1.1. Difference image analyses

Analyses of the full study area provided a general impression of the quality of synthetic reflectance and NDVI data produced by application of the STARFM algorithm to semi-arid rangeland. Pixel-based analysis of area-wide difference images demonstrated STARFM's ability to produce accurate reflectance estimates on a 0–1 scale. MAEs were typically $\leq$0.10, for the red and NIR bands, regardless of the base input pair (Table 1). Reflectance estimates associated with the red band were, with few exceptions, less biased than associated NIR estimates, and always more precise (Table 1).

The accuracy and precision of predicted red reflectance values tended to decrease as the time lag between base and prediction dates increased. MAE values were typically less than 0.05 (median = 0.036; range = 0.015–0.063), while error standard deviation values never exceeded 0.05 (median = 0.030; range = 0.019–0.043) (Table 1). Neither the inputs used nor the time lag between the base pair and prediction dates influenced prediction bias for the 06 June and 09 August base pairs. All predictions based on the 22 June base pair were biased low and became more biased as the time lag between the input and prediction dates increased. All forecasts for the 26 September and 12 October prediction dates were biased low regardless of the base pair, and these two late season scenes consistently overestimated red reflectance values when hindcasting.

Synthetic NIR reflectance data consistently exhibited less accuracy and precision than their corresponding red reflectance predictions. MAE values (median = 0.065; range = 0.028–0.103) and error standard deviation values (median = 0.055; range = 0.030–0.085) increased, with few exceptions, as the lag between base and prediction date increased (Table 1). The time lag between base and prediction dates did not influence prediction bias (median = −0.000; range = −0.079 to 0.092); however, synthetic NIR scenes were typically biased low when forecasting, regardless of base pair. Similar to the red reflectance predictions, all forecasts for the 26 September and 12 October prediction dates were biased low for all base pairs, and these two late season scenes consistently overestimated NIR reflectance values when hindcasting.

The quality of NDVI estimates was less consistent than the synthetic reflectance data used to create them (Table 1). Accuracy tended to decrease for all input pairs as the lag between base and prediction dates increased. The first four base pairs, i.e., 06 June, 22 June, 09 August, and 26 September, produced accurate estimates for all prediction dates prior to 12 October (median = 0.075, range = 0.057–0.100); however bias was variable within base pair dates. Predictions for 22 June and 09 August were consistently biased low regardless of base pair while 12 October predictions were consistently biased high.

3.1.2. Correlation analyses

Pixel-based simple linear regression analyses (Table 2) revealed moderate to strong correlations between observed and predicted red reflectance data for all base and prediction date combinations

Table 1
Mean absolute error, mean error, and error standard deviation determined by full scene difference image analysis of observed and predicted surface reflectance and NDVI values. Analyses were not conducted for coincident base pair and prediction dates.

Base date	Data set	Prediction date													
		06 June			22 June			09 August			26 September			12 October		
		Mean absolute error	Mean error	Error SD	Mean absolute error	Mean error	Error SD	Mean absolute error	Mean error	Error SD	Mean absolute error	Mean error	Error SD	Mean absolute error	Mean error	Error SD
06 June	RED	–	–	–	0.027	0.025	0.019	0.025	0.019	0.027	0.031	−0.026	0.030	0.045	−0.041	0.039
	NIR	–	–	–	0.039	0.034	0.030	0.036	0.021	0.047	0.059	−0.049	0.056	0.080	−0.068	0.076
	NDVI	–	–	–	0.068	−0.050	0.078	0.084	−0.043	0.113	0.077	−0.002	0.114	0.091	0.029	0.125
22 June	RED	0.023	−0.020	0.019	–	–	–	0.015	−0.004	0.024	0.046	−0.044	0.031	0.055	−0.052	0.040
	NIR	0.034	−0.029	0.033	–	–	–	0.028	−0.007	0.044	0.080	−0.074	0.060	0.095	−0.079	0.085
	NDVI	0.073	0.048	0.085	–	–	–	0.062	−0.003	0.100	0.100	0.030	0.135	0.133	0.064	0.160
09 August	RED	0.021	−0.015	0.024	0.015	0.009	0.024	–	–	–	0.042	−0.040	0.026	0.052	−0.046	0.043
	NIR	0.032	−0.010	0.054	0.029	0.017	0.037	–	–	–	0.070	−0.068	0.044	0.082	−0.071	0.071
	NDVI	0.090	0.054	0.112	0.057	−0.005	0.092	–	–	–	0.070	0.033	0.096	0.117	0.059	0.145
26 September	RED	0.027	0.022	0.029	0.049	0.047	0.031	0.044	0.043	0.028	–	–	–	0.025	−0.016	0.030
	NIR	0.061	0.050	0.063	0.085	0.075	0.059	0.070	0.066	0.046	–	–	–	0.039	−0.022	0.047
	NDVI	0.078	−0.004	0.113	0.096	−0.062	0.120	0.072	−0.046	0.091	–	–	–	0.073	0.024	0.099
12 October	RED	0.041	0.037	0.036	0.063	0.062	0.041	0.060	0.059	0.040	0.020	0.012	0.025	–	–	–
	NIR	0.076	0.060	0.075	0.103	0.092	0.077	0.088	0.079	0.073	0.035	0.007	0.049	–	–	–
	NDVI	0.095	−0.037	0.130	0.114	−0.079	0.132	0.104	−0.072	0.127	0.065	−0.029	0.089	–	–	–

Table 2
Results of pixel-based correlation analysis of observed surface reflectance and NDVI measurements versus STARFM based predictions. Analyses were not conducted for coincident base pair and prediction dates.

Base date	Data set	Prediction date														
		06 June			22 June			09 August			26 September			12 October		
		Intercept	Slope	r^2	Intercept	Slope	r^2	Intercept	Slope	r^2	Intercept	Slope	r^2	Intercept	Slope	r^2
06 June	RED	–	–	–	0.02	1.03	0.89	0.04	0.83	0.76	0.02	0.63	0.76	0.03	0.42	0.58
	NIR	–	–	–	0.06	0.92	0.79	0.09	0.73	0.55	0.08	0.52	0.49	0.12	0.27	0.24
	NDVI	–	–	–	0.02	0.86	0.87	0.06	0.76	0.72	0.05	0.85	0.63	0.16	0.65	0.44
22 June	RED	−0.01	0.85	0.84	–	–	–	0.02	0.81	0.82	0.01	0.60	0.73	0.02	0.42	0.52
	NIR	0.03	0.76	0.71	–	–	–	0.06	0.74	0.60	0.07	0.46	0.42	0.12	0.24	0.13
	NDVI	0.05	0.99	0.84	–	–	–	0.05	0.88	0.79	0.04	0.96	0.60	0.16	0.75	0.35
09 August	RED	0.01	0.79	0.74	0.01	0.94	0.81	–	–	–	0.00	0.67	0.83	0.02	0.48	0.42
	NIR	0.06	0.72	0.43	0.08	0.77	0.68	–	–	–	0.04	0.60	0.69	0.10	0.36	0.32
	NDVI	0.13	0.82	0.71	0.07	0.84	0.82	–	–	–	0.04	0.99	0.76	0.14	0.78	0.42
26 September	RED	0.02	1.01	0.74	0.04	1.09	0.77	0.03	1.13	0.85	–	–	–	0.01	0.78	0.72
	NIR	0.07	0.93	0.45	0.10	0.89	0.48	0.05	1.05	0.70	–	–	–	0.06	0.70	0.70
	NDVI	0.11	0.75	0.68	0.07	0.73	0.69	0.05	0.77	0.82	–	–	–	0.08	0.84	0.64
12 October	RED	0.02	1.16	0.71	0.04	1.26	0.73	0.03	1.24	0.77	0.00	1.10	0.87	–	–	–
	NIR	0.09	0.89	0.35	0.12	0.89	0.35	0.07	1.03	0.47	−0.01	1.05	0.74	–	–	–
	NDVI	0.10	0.69	0.59	0.08	0.67	0.63	0.07	0.68	0.64	0.02	0.87	0.75	–	–	–

based on the coefficient of determination, R^2 (median = 0.76; range = 0.42–0.89); however, correlation strength decreased for all base dates as the time lag increased. R^2 values associated with NIR reflectance data (median = 0.48; range = 0.13–0.79) were usually lower than those associated with the red reflectance data and decreased as the time lag between base and prediction dates increased. Analysis of the red and NIR slope coefficients indicated, with few exceptions, greater departure from the 1:1 regression line as the lag between base and prediction dates increased.

Moderate to strong correlations (median = 0.69; range = 0.35–0.87) were evident for most sets of observed and predicted NDVI values (Table 2); however, R^2 values associated with each base date tended to decrease as the time lag between base and prediction dates increased. The degree of correlation associated with each prediction date generally decreased as the lag increased, but was remarkably low for 12 October regardless of base date. Prediction dates closest to each base pair tended to have intercept values approaching zero and slope coefficients that most strongly indicated a 1:1 relationship between the observed and predicted NDVI values.

3.2. Stratified NDVI predictions

3.2.1. Difference image analyses

Analysis of the entire study area provides a general impression of how well the STARFM algorithm performed when applied to semi-arid rangeland; however, analyses based on individual LCLU classes can reveal important similarities and differences among NDVI estimates that span a growing season (Table 3). The 22 June base pair produced estimates with accuracies typically <0.10 (median = 0.063; range = 0.036–0.102) across all LCLU classes for the two earliest prediction dates, but 26 September and 12 October predictions were generally less accurate across all classes (median = 0.123; range = 0.061–0.177). The sagebrush shrubland class produced the most accurate estimates for all prediction dates, while the least accurate estimates for the 06 June and 09 August prediction dates were associated with the pasture/hay class and the grassland class for the 26 September and 12 October prediction dates. Estimates associated with four LCLU classes were biased low for the 09 August prediction date; all other estimates were biased high regardless of LCLU or lag between base and prediction dates. Precision decreased for all LCLU classes as the lag between 22 June and the prediction date increased.

Comparison of the quality of NDVI predictions resulting from the use of a single base pair, 22 June, versus those based on the chronologically closest base pair revealed substantial differences. Use of the nearest date base pair produced more accurate and more precise estimates than when a single date was used as the base pair (Table 4). This was true for all LCLU classes and applied to both prediction dates, i.e., 26 September and 12 October. Predictions based on the nearest date base pair were always less biased for the 12 October prediction date; however, 26 September predictions were less consistent.

3.2.2. Correlation analyses

Pixel-based simple linear regression analysis (Table 5, Fig. 3) of 06 June and 09 August estimates revealed a strong correlation, $R^2 \geq 0.57$, between observed NDVI values and those predicted using the 22 June base pair. Correlation strength decreased as the time lag from 22 June increased and varied from moderate to high (median = 0.49; range = 0.31–0.59) and weak to moderate (median = 0.25; range = 0.10–0.37) for 26 September and 12 October prediction dates, respectively. All LCLU classes exhibited

Table 3
Mean absolute error, mean error, and error standard deviation determined by full scene difference image analysis of observed and predicted NDVI values stratified by land cover or land use (LCLU) classification. All predictions used a base pair date of 22 June.

Land cover/land use	Prediction date											
	06 June			09 August			26 September			12 October		
	Mean absolute error	Mean error	Error SD	Mean absolute error	Mean error	Error SD	Mean absolute error	Mean error	Error SD	Mean absolute error	Mean error	Error SD
Coniferous forest	0.088	0.076	0.073	0.054	−0.018	0.083	0.114	0.017	0.163	0.152	0.034	0.206
Deciduous forest	0.067	0.059	0.055	0.053	0.006	0.083	0.125	0.091	0.122	0.177	0.145	0.151
Deciduous shrubland	0.062	0.054	0.051	0.053	−0.002	0.079	0.101	0.056	0.115	0.161	0.120	0.150
Disturbed/modified	0.061	0.036	0.074	0.054	0.002	0.080	0.075	0.010	0.104	0.106	0.033	0.136
Grassland	0.072	0.055	0.075	0.072	0.036	0.095	0.130	0.095	0.134	0.155	0.107	0.159
Mixed forest	0.084	0.079	0.059	0.053	0.015	0.074	0.125	0.088	0.124	0.165	0.120	0.157
Pasture/hay	0.088	0.046	0.109	0.102	−0.020	0.143	0.118	0.024	0.163	0.128	0.022	0.168
Riparian/wetland	0.082	0.059	0.090	0.084	−0.019	0.124	0.116	0.036	0.158	0.137	0.063	0.170
Sagebrush shrubland	0.053	0.030	0.063	0.036	0.000	0.054	0.061	0.001	0.084	0.099	0.043	0.122
Steppe	0.064	0.045	0.067	0.046	0.005	0.068	0.086	0.029	0.111	0.122	0.072	0.138

Table 4
Comparison of the performance of predictions based on a single base date versus use of the nearest preceding date. Mean absolute error, mean error, and error standard deviation were determined by full scene difference image analysis of observed and predicted NDVI values stratified by land cover or land use classification. All predictions based on a single date used a base pair date of 22 June. Base pair images collected on 09 August and 26 September were used to calculate predictions on 26 September and 12 October, respectively.

Land cover/land use	Prediction date											
	26 September						12 October					
	Single date			Nearest date			Single date			Nearest date		
	Mean absolute error	Mean error	Error SD	Mean absolute error	Mean error	Error SD	Mean absolute error	Mean error	Error SD	Mean absolute error	Mean error	Error SD
Coniferous forest	0.114	0.017	0.163	0.092	0.031	0.124	0.152	0.034	0.206	0.087	−0.009	0.116
Deciduous forest	0.125	0.091	0.122	0.101	0.066	0.108	0.177	0.145	0.151	0.106	0.072	0.111
Deciduous shrubland	0.101	0.056	0.115	0.079	0.049	0.091	0.161	0.120	0.150	0.112	0.083	0.111
Disturbed/modified	0.075	0.010	0.104	0.049	0.016	0.070	0.106	0.033	0.136	0.072	−0.007	0.100
Grassland	0.130	0.095	0.134	0.081	0.052	0.097	0.155	0.107	0.159	0.084	0.021	0.112
Mixed forest	0.125	0.088	0.124	0.097	0.046	0.117	0.165	0.120	0.157	0.094	0.029	0.117
Pasture/hay	0.118	0.024	0.163	0.088	0.048	0.108	0.128	0.022	0.168	0.068	0.017	0.091
Riparian/wetland	0.116	0.036	0.158	0.088	0.052	0.111	0.137	0.063	0.170	0.071	0.035	0.097
Sagebrush shrubland	0.061	0.001	0.084	0.039	0.016	0.052	0.099	0.043	0.122	0.051	0.014	0.075
Steppe	0.086	0.029	0.111	0.055	0.030	0.070	0.122	0.072	0.138	0.060	0.025	0.082

Table 5
Results of pixel-based correlation analysis of observed NDVI estimates versus STARFM based predictions stratified by land cover or land use (LCLU) classification. All predictions use a base pair date of 22 June.

Land cover/land use	Prediction date											
	06 June			09 August			26 September			12 October		
	Intercept	Slope	r^2	Intercept	Slope	r^2	Intercept	Slope	r^2	Intercept	Slope	r^2
Coniferous forest	0.01	1.12	0.89	0.02	0.94	0.86	0.03	0.97	0.59	0.19	0.71	0.37
Deciduous forest	0.08	0.98	0.85	0.10	0.87	0.76	0.15	0.88	0.49	0.30	0.65	0.18
Deciduous shrubland	0.06	0.99	0.87	0.07	0.88	0.78	0.10	0.90	0.49	0.24	0.71	0.10
Disturbed/modified	0.04	1.00	0.75	0.05	0.85	0.72	0.02	0.97	0.49	0.20	0.54	0.16
Grassland	0.05	1.02	0.86	0.07	0.93	0.78	0.04	1.13	0.58	0.19	0.80	0.24
Mixed forest	0.12	0.94	0.75	0.13	0.83	0.74	0.19	0.83	0.44	0.28	0.71	0.31
Pasture/hay	0.14	0.83	0.68	0.14	0.69	0.57	0.16	0.68	0.31	0.27	0.42	0.12
Riparian/wetland	0.10	0.92	0.81	0.09	0.79	0.65	0.09	0.86	0.46	0.21	0.62	0.27
Sagebrush shrubland	0.03	0.98	0.74	-0.01	1.02	0.68	−0.02	1.12	0.42	0.08	0.86	0.27
Steppe	0.02	1.05	0.84	0.01	0.99	0.81	−0.04	1.23	0.55	0.08	0.98	0.25

a decline in correlation strength between observed and predicted values as the lag between base pair and prediction dates increased. Associated slope coefficients tended to show greater departure from unity as the time lag increased; however, several LCLU classes had slope coefficients associated with the 26 September prediction date that approached unity. Intercept values demonstrated an increased departure from zero as the lag between base and prediction date increased, with few exceptions. Base input pair selection influenced the quality of the stratified NDVI estimates (Table 6). Pixel-based correlation analyses using the chronologically closest base pair, rather than the 22 June base date, always produced stronger correlation values for the 26 September and 12 October prediction dates. The nearest input date also produced slope coefficients that were closer to unity and intercept values that were closer to zero than those associated with the 12 October prediction date. This also held true, with two exceptions, for the 26 September prediction date.

4. Discussion and conclusions

Sequential down-scaled surface reflectance and NDVI estimates provide an effective means of monitoring plant phenology and biomass associated with diverse biomes (Hilker et al., 2009a; Hwang et al., 2011; Singh, 2012), but efforts to evaluate the quality of these synthetic products and their application to semi-arid rangeland have been limited (Kim and Hogue, 2012; Schmidt et al., 2012; Walker et al., 2012). We provide a rigorous assessment of data produced by the application of the STARFM algorithm to a suite of LCLU classes important to managers of semi-arid rangeland in the western United States. Analysis of the suite of synthetic Landsat product time-series revealed that the STARFM algorithm produces accurate predictions when applied to semi-arid rangeland, but input pair selection and the time lag between input and prediction dates influence the quality of reflectance and NDVI estimates.

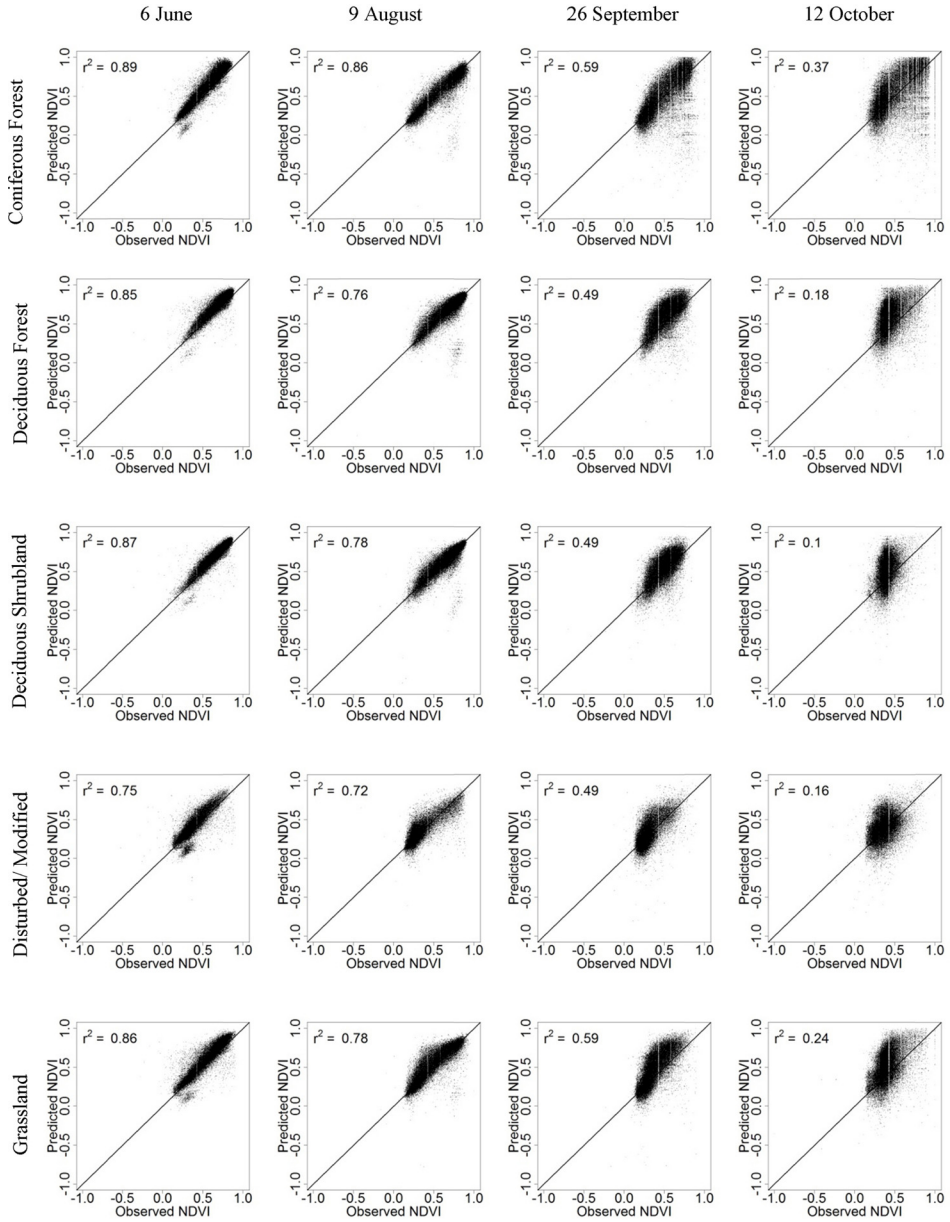

Fig. 3. Per-pixel comparison of observed and predicted NDVI values stratified by land cover or land use (LCLU). Rows show the change in correlation over the growing season, and columns depict the prediction dates. All predictions use a base pair date of 22 June 2006. Stronger correlations occurred early in the growing season, regardless of LCLU. The coefficients of determination are based on the entire LCLU classification. A sample of 50,000 points is displayed for each LCLU.

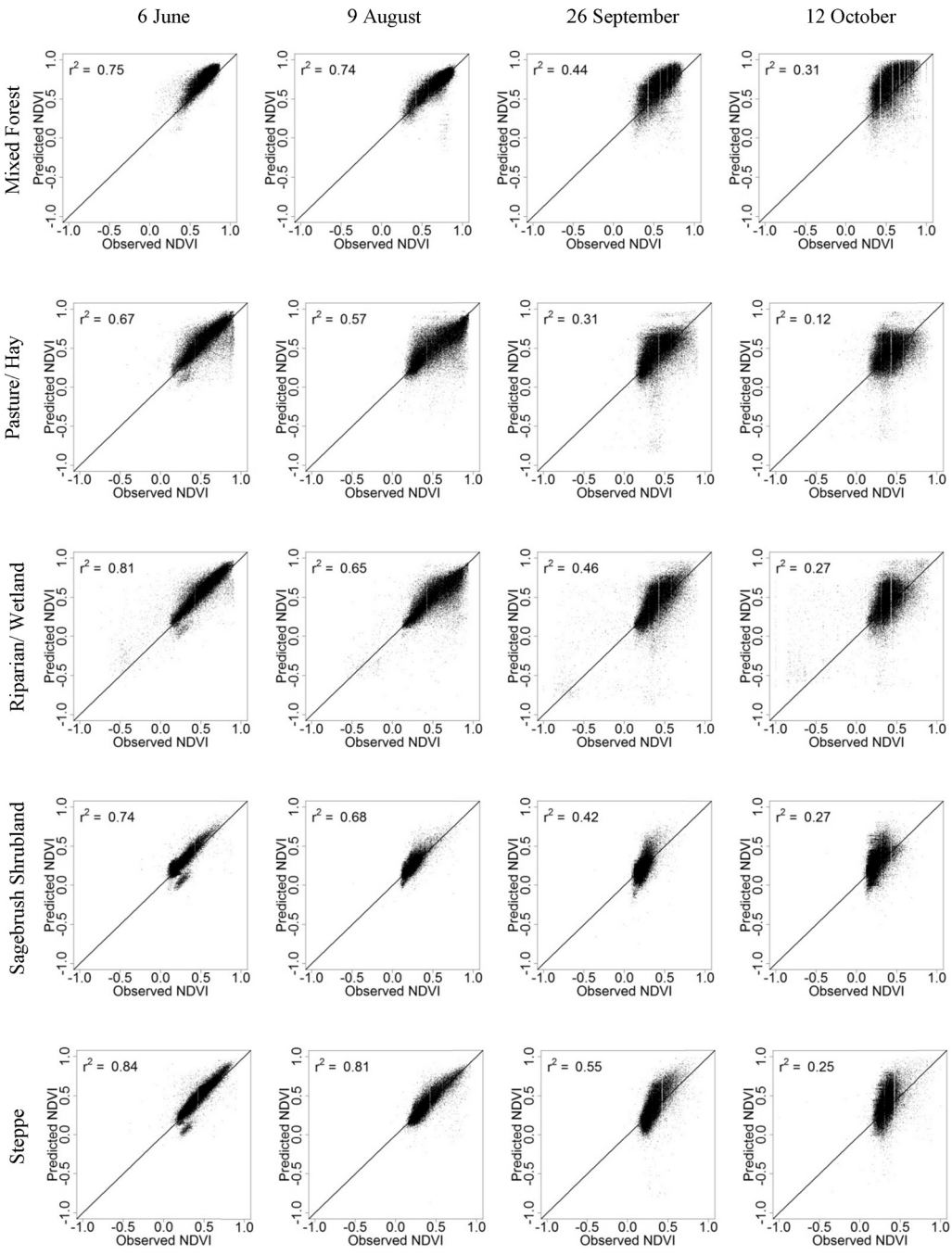

Fig. 3. (*Continued.*)

Red reflectance predictions demonstrated consistently greater accuracy and stronger correlation with known values when compared to their associated NIR predictions. This relationship held true regardless of the input pair date or the duration of the lag. These findings differed from previous studies that attributed better NIR (Hilker et al., 2009b; Roy et al., 2008) and short-wave infrared (Liu and Weng, 2012) predictions to greater influence of atmospheric contamination on shorter wavelengths; however, they were similar to results associated with semi-arid dryland forest (Walker et al., 2012). We caution that the relative magnitude of band specific inaccuracies is inconsistent and recommend that all synthetic reflectance products be evaluated prior to use as the influence of site specific conditions might be variable across the visible and NIR portions of the spectrum. The quality of both synthetic reflectance products declined as the lag time increased in contrast to the relatively constant performance demonstrated by dryland forest predictions (Walker et al., 2012). These differences could be due to greater phenological variation present across rangeland comprised of multiple LCLU classes compared to conifer dominated forestland. Variations in phenology among LCLU classes (Bradley and Mustard, 2008; Schmidt et al., 2012) likely leads to more heterogeneity in reflectance across an area at any one time.

Our findings contribute to the previously limited knowledge regarding the quality of NDVI predictions produced from synthetic reflectance data. The first study to assess the quality of NDVI estimates showed stronger correlation between observed and predicted values than was observed for the individual reflectance bands associated with conifer-dominated forest (Hilker et al., 2009b). Our results were more similar to those presented by the only other study predicting similar values in a semi-arid region;

Table 6
Comparison of the performance of predictions based on a single base date versus use of the nearest preceding date. Intercept, slope, and coefficient of determination values were determined by regression of predicted against known NDVI values stratified by land cover or land use (LCLU) classification. All predictions based on a single date used a base pair date of 22 June. Base pair images collected on 09 August and 26 September were used to calculate predictions on 26 September and 12 October, respectively.

Land cover/land use	Prediction date											
	26 September						12 October					
	Single date			Nearest date			Single date			Nearest date		
	Intercept	Slope	r^2	Intercept	Slope	r^2	Intercept	Slope	r^2	Intercept	Slope	r^2
Coniferous forest	0.03	0.97	0.59	0.00	1.07	0.76	0.19	0.71	0.37	0.13	0.74	0.71
Deciduous forest	0.15	0.88	0.49	0.07	0.98	0.60	0.30	0.65	0.18	0.20	0.71	0.34
Deciduous shrubland	0.10	0.90	0.49	0.05	0.99	0.64	0.24	0.71	0.10	0.11	0.93	0.26
Disturbed/modified	0.02	0.97	0.49	0.01	1.02	0.70	0.20	0.54	0.16	0.10	0.69	0.37
Grassland	0.04	1.13	0.58	0.01	1.12	0.72	0.19	0.80	0.24	0.07	0.88	0.43
Mixed forest	0.19	0.83	0.44	0.06	0.98	0.55	0.28	0.71	0.31	0.20	0.70	0.45
Pasture/hay	0.16	0.68	0.31	0.11	0.85	0.60	0.27	0.42	0.12	0.10	0.81	0.60
Riparian/wetland	0.09	0.86	0.46	0.10	0.88	0.65	0.21	0.62	0.27	0.12	0.77	0.64
Sagebrush shrubland	−0.02	1.12	0.42	0.01	1.01	0.60	0.08	0.86	0.27	0.07	0.79	0.47
Steppe	−0.04	1.23	0.55	0.01	1.08	0.69	0.08	0.98	0.25	0.06	0.90	0.45

NDVI values were more highly correlated than the contributing synthetic NIR values, but less correlated than the analogous red values (Walker et al., 2012). Our NDVI correlation values were higher than those associated with the NIR predictions in all but one instance, and were typically lower than those associated with the red reflectance values. NDVI estimates were consistently less accurate than the associated reflectance predictions and tended to become less accurate as the lag between base and prediction dates increased. Similar performance was noted for dryland forests (Walker et al., 2012) and reveals a potential limitation of dense NDVI prediction time-series based on a single base date. Application of an alternative downscaling model (Hong et al., 2011) to a semi-arid region consisting of upland vegetation and riparian wetlands revealed a similar decline in performance as the temporal gap between the initial and prediction dates increased (Kim and Hogue, 2012), but the uncertainty associated with dynamic vegetation conditions influenced prediction quality more than the duration of the temporal gap between selected images.

Prediction quality, in general, improved as the time lag between input and prediction dates decreased. These findings support the conclusion that the accuracy of STARFM predictions depends on the similarity between the base input pair and the prediction date (Walker et al., 2012; Zhu et al., 2010). Our results support previous findings that use of multiple base pairs can produce more accurate predictions (Gao et al., 2006; Zhu et al., 2010); however, we demonstrate that multiple individual base pairs can be applied sequentially as opposed to concurrently in the same prediction algorithm. The chronological order of the base and prediction dates did not influence bias; therefore, a time-series comprised of hindcast and forecast predictions developed using the chronologically closest base pair is likely to best capture spatial and temporal differences associated with phenology or changes in aboveground phytomass.

Expected differences in phenology and phytomass production among LCLU classes (Bradley and Mustard, 2008; Schmidt et al., 2012) motivated an examination of NDVI predictions stratified by class. The consistent quality of the NDVI estimates, preceding the 26 September and 12 October prediction dates, demonstrated that use of a single base pair date can produce accurate estimates across LCLU classes within a growing season and revealed the challenge of forecasting NDVI estimates beyond the growing season (Hilker et al., 2009b). Our single base pair approximated the peak of the growing season (Thoma, 2011), which could explain its robustness over the entire growing season; however, predictions based on the temporally closest available base pair resulted in more accurate and less biased estimates for both of the late season dates and provide further evidence of the importance of base pair selection (Walker et al., 2012).

Sagebrush grassland cover types provide important forage for wild and domestic ungulates and are often the focus of range monitoring and wildlife management actions because of the potential for foraging niche overlap (Hobbs et al., 1996; Torstenson et al., 2006). NDVI estimates associated with sagebrush shrubland were the most accurate modeled, closely approximated the 1:1 regression line, and demonstrated moderate to strong agreement with observed TM-derived NDVI values throughout the summer. The extensive distribution and uniformity of sagebrush stands likely provided the homogeneous coarse-resolution pixels required by the STARFM to produce accurate predictions (Gao et al., 2006). The pasture/hay LCLU class, in comparison, exhibited some of the largest errors, biggest departure from the 1:1 regression line, and lowest correlations over the growing season. Prediction errors were likely influenced by a relatively small patch size, heterogeneity associated with forage offtake due to grazing and mowing, and extreme NDVI values due to spatially variable irrigation. Compared to the pasture/hay class, the grassland class, which was likely composed of similar native herbaceous vegetation growing under more natural grazing and moisture regimes, showed a stronger correlation between observed and predicted values, less departure from the 1:1 regression line, and more accurate estimates throughout the growing season. These results indicate a need to further evaluate the impact of the type and timing of management actions, e.g., irrigation, haying, and grazing, on the accuracy of synthetic Landsat data as such activities could produce small patches with extreme values that are often associated with larger prediction errors (Gao et al., 2006).

Predictions associated with the conifer class were less accurate and exhibited greater deviation from the 1:1 regression line, especially in late fall, than was expected for a wide-spread cover type that occurs in large, nearly monotypic stands. Prediction quality was similar to or lower than other cover types, e.g., deciduous and mixed forest, deciduous shrubland, and riparian and wetland areas, known to occur as small patches or within phenologically heterogeneous areas. Mortality associated with the mountain pine beetle (*Dendroctonus ponderosae*) might have lead to within-stand heterogeneity due to the live/dead tree mosaic. Signs of infestation can manifest over several years, lead to changes in reflectance over the growing season (Safranyik and Wilson, 2006; Wulder et al., 2006), and produce spectral dissimilarity within a cover type. Such fine grained disturbances will be difficult to model until contiguous areas coalesce into larger regions with similar spectral properties.

The results of this study suggest that land managers of semi-arid rangelands might have alternatives when it comes to the assessment and monitoring of the phytomass component of rangelands. The recent success of the Landsat Data Continuity Mission (U.S.

Geological Survey, 2012) provides the possibility of even higher quality predictions based on Landsat 8 imagery. Data collected by the Operational Land Imager sensor should be radiometrically and spectrally superior to that collected by Landsat 5's degraded Thematic Mapper sensor and provide more complete coverage than Landsat 7's recent SLC-off products. Additional work should examine the quality of synthetic Landsat data as they relate to specific habitat management actions and the timing of these activities. Our work confirms that use of STARFM can reliably model rangeland NDVI estimates; however results need validation to ensure estimates are of the proper spatiotemporal scale to adequately assess and monitor rangeland conditions. Linking in situ biomass and phenology measurements with STARFM based predictions could provide a framework for effectiveness monitoring of habitat treatments at fine to moderate spatial and temporal resolutions and broad spatial extents.

Acknowledgements

We thank the U.S. Geological Survey, the National Park Service, and the Bureau of Land Management for funding of this research. Ms. Rebecca Blenkner provided valuable image processing and GIS support. We thank Geneva Chong, Peter Gogan, Megan Higgs, and two anonymous reviewers for their helpful comments. Any use of trade, product, or firm names is for descriptive purposes only and does not imply endorsement by the U.S. Government.

References

Andelman, S., Gillem, K., Groves, C., Hansen, C., Humke, J., Klahr, T., Kramme, L., Moseley, B., Reid, M., Vander Schaaf, D., Coad, M., DeForest, C., Macdonald, C., Baumgarther, J., Hak, J., Hobbs, S., Lunte, L., Smith, L., Soper, C., 1999. The Columbia Plateau Ecoregional Assessment: A Pilot Effort in Ecoregional Conservation. The Nature Conservancy, Seattle, Washington.

Bailey, R.G., 1995. Description of the Ecoregions of the United States, second ed. U.S. Department of Agriculture, Forest Service, Washington, DC.

Blanco, L.J., Ferrando, C.A., Biurrun, F.N., 2009. Remote sensing of spatial and temporal vegetation patterns in two grazing systems. Rangeland Ecology and Management 62, 445–451.

Booth, D.T., Tueller, P.T., 2003. Rangeland monitoring using remote sensing. Arid Land Research and Management 17, 455–467.

Bradley, B.A., Mustard, J.F., 2008. Comparison of phenology trends by land cover class: a case study in the Great Basin, USA. Global Change Biology 14, 334–346.

Bradley, B.A., O'Sullivan, M.T., 2011. Assessing the short-term impacts of changing grazing regime at the landscape scale with remote sensing. International Journal of Remote Sensing 32, 5797–5813.

Chander, G., Markham, B.L., Helder, D.L., 2009. Summary of current radiometric calibration coefficients for Landsat MSS, TM, ETM+, and EO-1 ALI sensors. Remote Sensing of Environment 113, 893–903.

Chavez Jr., P.S., 1996. Image-based atmospheric corrections – revisited and improved. Photogrammetric Engineering and Remote Sensing 62, 1025–1036.

Comer, P., Faber-Langendoen, D., Evans, R., Gawler, S., Josse, C., Kittel, G., Menard, S., Pyne, M., Reid, M., Schulz, K., Snow, K., Teague, J., 2003. Ecological systems of the United States: a working classification of U.S. terrestrial systems. NatureServe, Arlington, VA.

Coops, N.C., Hilker, T., Bater, C.W., Wulder, M.A., Nielsen, S.E., McDermid, G., Stenhouse, G., 2012. Linking ground-based to satellite-derived phenological metrics in support of habitat assessment. Remote Sensing Letters 3, 191–200.

Eisfelder, C., Kuenzer, C., Dech, S., 2012. Derivation of biomass information for semi-arid areas using remote-sensing data. International Journal of Remote Sensing 33, 2937–2984.

Emelyanova, I.V., McVicar, T.R., Van Niel, T.G., Li, L.T., van Dijk, A.I.J.M., 2012. On Blending Landsat-MODIS Surface Reflectances in Two Landscapes with Contrasting Spectral, Spatial and Temporal Dynamics. WIRADA Project 3.4: Technical Report. CSIRO Water for a Healthy Country Flagship, Australia.

Fernandez-Gimenez, M.E., McClaran, S.J., Ruyle, G., 2005. Arizona permittee and land management agency employee attitudes toward rangeland monitoring by permittees. Rangeland Ecology and Management 58, 344–351.

Freilich, J., Budd, B., Kohley, T., Hayden, B., 2001. The Wyoming Basins Ecoregional Plan. The Nature Conservancy-Wyoming Field Office, Lander, Wyoming.

Gao, F., Masek, J., Schwaller, M., Hall, F., 2006. On the blending of the Landsat and MODIS surface reflectance: predicting daily Landsat surface reflectance. Transactions on Geoscience and Remote Sensing 44, 2207–2218.

GDAL, 2011. GDAL-Geospatial Data Abstraction Library: Version 1.9.0. Open Source Geospatial Foundation, http://download.osgeo.org/gdal

Hagen, S.C., Heilman, P., Marsett, R., Torbick, N., Salas, W., van Ravensway, J., Qi, J., 2012. Mapping total vegetation cover across western rangelands with moderate-resolution imaging spectroradiometer data. Rangeland Ecology and Management 65, 456–467.

Hansen, M.C., Roy, D.P., Lindquist, E., Adusei, B., Justice, C.O., Altstatt, A., 2008. A method for integrating MODIS and Landsat data for systematic monitoring of forest cover and change in the Congo Basin. Remote Sensing of Environment 112, 2495–2513.

Hijmans, R.J., van Etten, J., 2011. raster: Geographic analysis and modeling with raster data. R package version 1.9-44, http://CRAN.R-project.org/package=raster

Hilker, T., Wulder, M.A., Coops, N.C., Linke, J., McDermid, G., Masek, J.G., Gao, F., White, J.C., 2009a. A new data fusion model for high spatial- and temporal-resolution mapping of forest disturbance based on Landsat and MODIS. Remote Sensing of Environment 113, 1613–1627.

Hilker, T., Wulder, M.A., Coops, N.C., Seitz, N., White, J.C., Gao, F., Masek, J.G., Stenhouse, G., 2009b. Generation of dense time series synthetic Landsat data through data blending with MODIS using a spatial and temporal adaptive reflectance fusion model. Remote Sensing of Environment 113, 1988–1999.

Hobbs, N.T., Baker, D.L., Bear, G.D., Bowden, D.C., 1996. Ungulate grazing in sagebrush grassland: mechanisms of resource competition. Ecological Applications 6, 200–217.

Hong, S.-H., Hendrickx, J.M.H., Borchers, B., 2011. Down-scaling of SEBAL derived evapotranspiration maps from MODIS (250 m) to Landsat (30 m) scales. International Journal of Remote Sensing 32, 6457–6477.

Huete, A., Didan, K., Miura, T., Rodriguez, E.P., Gao, X., Ferreira, L.G., 2002. Overview of the radiometric and biophysical performance of the MODIS vegetation indices. Remote Sensing of Environment 83, 195–213.

Hunt Jr., E.R., Everitt, J.H., Ritchie, J.C., Moran, M.S., Booth, D.T., Anderson, G.L., Clark, P.E., Seyfried, M.S., 2003. Applications and research using remote sensing for rangeland management. Photogrammetric Engineering and Remote Sensing 69, 675–693.

Hunt Jr., E.R., Miyake, B.A., 2006. Comparison of stocking rates from remote sensing and geospatial data. Rangeland Ecology and Management 59, 11–18.

Hwang, T., Song, C., Bolstad, P.V., Band, L.E., 2011. Downscaling real-time vegetation dynamics by fusing multi-temporal MODIS and Landsat NDVI in topographically complex terrain. Remote Sensing of Environment 115, 2499–2512.

James, L.F., Young, J.A., Sanders, K., 2003. A new approach to monitoring rangelands. Arid Land Research and Management 17, 319–328.

Jensen, J.R., 1983. Biophysical remote sensing. Annals of the Association of American Geographers 73, 111–132.

Ju, J., Roy, D.P., 2008. The availability of cloud-free Landsat ETM+ data over the conterminous United States and globally. Remote Sensing of Environment 112, 1196–1211.

Kennedy, R.E., Townsend, P.A., Gross, J.E., Cohen, W.B., Bolstad, P., Wang, Y.Q., Adams, P., 2009. Remote sensing change detection tools for natural resource managers: understanding concepts and tradeoffs in the design of landscape monitoring projects. Remote Sensing of Environment 113, 1382–1396.

Kerr, J.T., Ostrovsky, M., 2003. From space to species: ecological applications for remote sensing. Trends in Ecology and Evolution 18, 299–305.

Kim, J., Hogue, T.S., 2012. Evaluation and sensitivity testing of a coupled Landsat-MODIS downscaling method for land surface temperature and vegetation indices in semi-arid regions. Journal of Applied Remote Sensing 6, 1–17.

Liu, H., Weng, Q., 2012. Enhancing temporal resolution of satellite imagery for public health studies: a case study of West Nile Virus outbreak in Los Angeles in 2007. Remote Sensing of Environment 117, 57–71.

Millennium Ecosystem Assessment, 2005. Ecosystems and Human Well-being: Synthesis. Island Press, Washington, DC.

Nachlinger, J., Sochi, K., Comer, P., Kittel, G., Dorfman, D., 2001. Great Basin: An Ecoregion-based Conservation Blueprint. The Nature Conservancy, Reno, NV.

National Research Council, 1994. Rangeland Health: New Methods to Classify, Inventory, and Monitor Rangelands. The National Academies Press, Washington, DC.

Nickerson, C., Ebel, R., Borchers, A., Carriazo, F., 2011. Major Uses of Land in the United States, 2007, EIB-89. United States Department of Agriculture, Economic Research Service.

Noss, R., Wuerthner, G., Vance-Borland, K., Carroll, C., 2001. A Biological Conservation Assessment for the Utah-Wyoming Rocky Mountains Ecoregion. Conservation Science Inc., Corvallis, OR.

Pickup, G., Chewings, V.H., 1994. A grazing gradient approach to land degradation assessment in arid areas from remotely-sensed data. International Journal of Remote Sensing 15, 597–617.

Pohl, C., van Genderen, J.L., 1998. Multisensor image fusion in remote sensing: concepts, methods and applications. International Journal of Remote Sensing 19, 823–854.

PRISM Climate Group, 2007. 2006 Annual Total Precipitation. Oregon State University, Created May 14, 2007. http://prism.oregonstate.edu (accessed 17.09.2012).

R Development Core Team, 2011. R: A Language and Environment for Statistical Computing. R Foundation for Statistical Computing, Vienna, Austria, URL http://www.R-project.org/

Ramsey, R.D., Wright Jr., D.L., McGinty, C., 2004. Evaluating the use of Landsat 30 m enhanced thematic mapper to monitor vegetation cover in shrub-steppe environments. Geocarto International 19, 39–47.

Rouse Jr., J.W., Haas, R.H., Schell, J.A., Deering, D.W., 1974. Monitoring vegetation systems in the great plains with ERTS. In: Third Earth Resources Technology Satellite-1 Symposium, NASA, Washington, DC, pp. 309–317.

Rowland, M.M., Leu, M., 2011. Chapter 1: study area description. In: Hanser, S.E., Leu, M., Knick, S.T., Aldridge, C.L. (Eds.), Sagebrush Ecosystem Conservation and

Management: Ecoregional Assessment Tools and Models for the Wyoming Basins. Allen Press Inc., Lawrence, KS, pp. 10–45.
Roy, D.P., Ju, J., Lewis, P., Schaaf, C., Gao, F., Hansen, M., Lindquist, E., 2008. Multi-temporal MODIS-Landsat data fusion for relative radiometric normalization, gap filling, and prediction of Landsat data. Remote Sensing of Environment 112, 3112–3130.
Safranyik, L., Wilson, B., 2006. The Mountain Pine Beetle: A Synthesis of Biology, Management, and Impacts on Lodgepole Pine. Canadian Forest Service, Victoria, British Columbia.
Schmidt, M., Udelhoven, T., Gill, T., Roder, A., 2012. Long term data fusion for a dense time series analysis with MODIS and Landsat imagery in an Australian Savanna. Journal of Applied Remote Sensing 6, 1–18.
Singh, D., 2011. Generation and evaluation of gross primary productivity using Landsat data through blending with MODIS data. International Journal of Applied Earth Observation and Geoinformation 13, 59–69.
Singh, D., 2012. Evaluation of long-term NDVI time series derived from Landsat data through blending with MODIS data. Atmosfera 25, 43–63.
Švab, A., Oštir, K., 2006. High-resolution image fusion: methods to preserve spectral and spatial resolution. Photogrammetric Engineering and Remote Sensing 72, 565–572.
Thoma, D.P., 2011. Remote Sensing of Vegetation Phenology and Snow-cover Extent in Northern Colorado Plateau Network Parks: Status and Trends 2010. Natural Resource Technical Report NPS/NCPN/NRTR-2011/455. National Park Service, Fort Collins, CO.
Torstenson, W.L.F., Mosley, J.C., Brewer, T.K., Tess, M.W., Knight, J.E., 2006. Elk, mule deer, and cattle foraging relationships on foothill and mountain rangeland. Rangeland Ecology and Management 59, 80–87.
Tueller, P.T., 1989. Remote sensing technology for rangeland management applications. Journal of Range Management 42, 442–453.
Turner, W., Spector, S., Gardiner, N., Fladeland, M., Sterling, E., Steininger, M., 2003. Remote sensing for biodiversity science and conservation. Trends in Ecology and Evolution 18, 306–314.
U.S. Geological Survey, 2012. Landsat Data Continuity Mission: U.S. Geological Survey Fact Sheet 2012–3066. U.S. Department of the Interior, pp. 4 (Revised July 18, 2012).
Walker, J.J., de Beurs, K.M., Wynne, R.H., Gao, F., 2012. Evaluation of Landsat and MODIS data fusion products for analysis of dryland forest phenology. Remote Sensing of Environment 117, 381–393.
Washington-Allen, R.A., West, N.E., Ramsey, R.D., Efroymson, R.A., 2006. A protocol for retrospective remote sensing-based ecological monitoring of rangelands. Rangeland Ecology and Management 59, 19–29.
West, N.E., 2003. History of rangeland monitoring in the U.S.A. Arid Land Research and Management 17, 495–545.
Wulder, M.A., Dymond, C.C., White, J.C., Leckie, D.G., Carroll, A.L., 2006. Surveying mountain pine beetle damage of forests: a review of remote sensing opportunities. Forest Ecology and Management 221, 27–41.
Wulder, M.A., White, J.C., Goward, S.N., Masek, J.G., Irons, J.R., Herold, M., Cohen, W.B., Loveland, T.R., Woodcock, C.E., 2008. Landsat continuity: issues and opportunities for land cover monitoring. Remote Sensing of Environment 112, 955–969.
Zhu, X., Chen, J., Gao, F., Chen, X., Masek, J.G., 2010. An enhanced spatial and temporal adaptive reflectance fusion model for complex heterogeneous regions. Remote Sensing of Environment 114, 2610–2623.